Performance Analysis of Fiber Fault PON Monitoring Using Optical Coding: SNR, SNIR, and False-Alarm Probability

Mohammad M. Rad, *Member, IEEE,* Habib A. Fathallah, *Member, IEEE,* and Leslie A. Rusch, *Felow, IEEE*

***Abstract*—We evaluate the theoretical performance of recently proposed optical coding (OC) technology for fiber fault monitoring of a PON through the signal-to-noise ratio (SNR), the signal-to-noise-plus-interference ratio (SNIR), and the false-alarm probability. First, we develop a mathematical model and expressions for the detected monitoring signals considering a square law detector and using realistic parameters. Second, we address the effect of the transmitted pulse power, network size and light source coherence on the performance of both one-dimensional (1D) and two-dimensional (2D) OC monitoring systems. We show that the transmitted pulse width can be optimized to trade-off the interference and the detection noises. We give simple analytic equations for this optimal pulse width as a function of network parameters. Both 1D and 2D coding schemes are considered. We find that, under perfect dispersion compensation, an incoherent source performs better than lasers for 1D coding. In addition, 2D coding using lasers offer very good performance and supports networks up to 128 customers with SNIR$\geq$10dB; a promising candidate for future high capacity PON. Finally, we apply Neyman-Pearson testing to the receiver of our monitoring system and investigate how coding and network size affect the operational expenses (OPEX) of our monitoring system.**

***Index Terms*—False-alarm probability (P_{FA}), network monitoring, PON, OTDR, OCDMA, optical coding (OC), signal-to-noise-ratio (SNR), signal-to-noise-plus-interference ratio (SNIR).**

I. Introduction

OPTICAL-time-domain reflectometry (OTDR) is efficient for testing optical devices and fiber link monitoring of point-to-point (PTP) networks; however it has yet to demonstrate its full applicability for point-to-multipoint (PMP) networks like FTTH-PONs [1-7]. It is difficult for the central office (CO) network manager to identify a specific broken fiber branch in a tree architecture PON. Two monitoring strategies exist that tend to address this problem: centralized and distributed. The first provides the CO the ability to acquire remotely, live, in-service, full information about the network. The second considers placing active modules inside the optical network terminations (ONTs) responsible for making performance measurements, and sending the information up to the CO. This approach is an effective tool for preventive maintenance of the fiber link, however it falls idle when abrupt interruption occurs in a distribution/drop fiber (DDF), i.e., when monitoring is most critical.

A few centralized techniques have been previously proposed for in-service PON management [8-13]; all are impractical due to their limited capacity (maximum of a few dozen of customers). In this paper, we consider a centralized strategy for fiber link monitoring of a PON that exploits passive optical code division multiplexing (OCDM) technology. In [6], we introduced, for the first time, the use of a modified OCDM scheme for centralized fiber link monitoring of architecture agnostic PONs. In [7], we developed a mathematical framework for this monitoring system and derived closed form expressions for the interference probability and the signal-to-interference ratio (SIR). We demonstrated the importance of geographical distribution and the transmitted pulse duration on the system performance measured in terms of SIR for five geographic distributions for the PON topology. Reducing the transmitted pulse duration improves the SIR proportionally. However, decreasing the pulse width also decreases the received energy, creating new dominant noise effects not investigated in [7]. This paper extends our analysis by evaluating the overall performance of the system using signal-to-noise ratio (SNR), signal-to-noise-plus-interference ratio (SNIR), and the false-alarm probability (P_{FA}). Results from [7] will be applied directly to account for interference. We also address how design parameters such as power, pulse width, coding scheme, and source type affect the overall system performance.

In Section II, we briefly introduce the optical coding (OC) monitoring principle, summarize the key results previously obtained in [7], and develop the mathematical model of the detected signal taking into account all known interference and noise sources. In Section III, we address the beat noise and relative intensity noise in our system. We highlight and compare important differences between our monitoring system and standard optical CDMA data communication. Analytical expressions are derived for the different noise terms for both 1D (time only) and 2D (time $\times$ wavelength) coding schemes, each for coherent and incoherent light source. In Section IV, we define figures of merit SNIR and SNR for our monitoring

Paper approved by W. C. Kwong, the Editor for Optical Networks of the IEEE Communications Society. Manuscript received November 12, 2008; revised June 18, 2009 and October 16, 2009.

M. M. Rad and L. A. Rusch are with the Department of Electrical and Computer Engineering, Laval University, Quebec, Canada. They are also with the Center of Optics, Photonics, and Laser (COPL) (e-mail: mohammad.mansouri-rad.1@ulaval.ca, rusch@gel.ulaval.ca).

H. A. Fathallah is with the Electrical Engineering Department, College of Engineering, King Saud University, Riyadh, KSA, and is an adjunct professor with the Electrical and Computer Engineering Department, Laval University, Quebec, Canada (e-mail: hfathallah@ksu.edu.sa).

Digital Object Identifier 10.1109/TCOMM.2010.04.080504

system. Numerical results are then given to study the effects of transmitted power, and network size. In section V, we address the importance of transmitted pulse width on SNIR. In section VI we focus on the false-alarm probability, P_{FA}, and apply Neyman-Pearson hypothesis testing to our monitoring receiver. Finally, we offer concluding remarks in Section VII.

II. OCDM Monitoring System

A. Principle

In Fig. 1, we illustrate the principle of our OC based PON monitoring [6,7]. We differentiate each DDF in the PON using a specific optical encoder placed at the DDF end. The CO transmits an optical pulse, duration T_c, in the monitoring U band (1625-1675 nm). The pulse is split at the remote node (RN) passive splitter (PS) into subpulses, one traveling in each DDF. The monitoring subpulses are separated from the data signal at the front of ONT by a U band wavelength selector (WS); it is then coded and reflected back to the CO by a dual function device encoder/reflector, we call a coding mirror (CM_i, $i = 1, 2, \cdots, K$). The CO receives the sum of all the encoded signals returned by the CMs and extracts the information about a particular DDF by cyclically matching its unique decoder to the received signal. Features of the auto-correlation peak are used to assess the quality of the individual fiber link. If all network components are working well, the monitoring quality (auto-correlation peak) should be good. Otherwise one or more problems exist in the network. Our focus in this paper is on DDF status, i.e., faulty (with a break) or healthy (with no break) situations. The DDF status is then modeled by a Bernoulli random variable. When a break happens for a DDF, no encoding occurs and no auto-correlation peak is observed for that particular DDF. However, cross-correlation spikes and detection noises may cause errors in estimating the status of a particular DDF. The capacity of our monitoring technology is ultimately limited by the code family used, but orders of magnitude larger than previously proposed techniques [8-13].

Fig.1 shows two implementations of a 2D (1D) CM. A generic 2D (1D) CM passive splitter implementation using tapped delay lines (TDLs), bandpass filters (BPFs) and passive splitters/combiners (PSCs) and a circulator is illustrated [7]. A more practical, multiple-FBG (MFBG) implementation is also illustrated. Each grating in this structure reflects a different wavelength in a specific time (i.e., discrete position), corresponding to a preset 2D code. We consider 1D coding as a special case of 2D coding; all the gratings are tuned to reflect the same wavelength and no BPF is required. The FBG implementation obviates U band WS at the DDF ends as well as the additional circulator at CM; hence, reducing the component count and the total CM loss. Fig.1 also details the OCDM monitoring block. The same technology is considered for the decoding operation at the CO. The insertion loss of optical switches and BPFs are neglected. Recall that no continuous data transmission exists for our monitoring application. Hence, one photodetector is sufficient for the entire network. Depending on the desired DDF to be monitored, the optical switch selects the corresponding decoder, i.e., one customer is monitored at a time [7]. In subsection C we address the power/loss budget of each implementation.

B. Interference Statistics

In [7] we focused on the interference statistics and showed that interference depends on both the properties of the code family and the geographical distribution of the clients as well as the transmitted pulse width T_c. We demonstrated that our system suffers less from interference than optical code division multiple access (OCDMA) systems, as only very close undesired CMs, i.e., closer than the *correlation distance* l_{CD}, can contribute in the total decoded signal. We found $l_{CD} = cFT_c/2$ where F and c denote the time domain code length and the light velocity in the fiber core. We show that decreasing T_c is a good strategy to improve SIR. However, in real situations this creates new dominant noises which are to be investigated in this paper. We defined an i.i.d Bernoulli random sequence ρ_k, $k = 2, 3, \cdots, K$ (the first client represents the desired one, without loss of generality); $\rho_k = 1$ when customer k contributes non-zero interference. As indicated, the DDF status is modeled by a Bernoulli random variable $\xi_k \in \{0, 1\}$ which is assumed to be the same for all DDFs. We considered a family of multi-wavelength optical orthogonal codes (MW-OOCs) with $(F, M, w = 4, \lambda_a = \lambda_c = 1)$ where M, w, λ_a and λ_c are the available number of wavelengths, code weight, maximum of (out-of-phase) auto and cross correlation values, respectively. The code length F is related to the network size K [14],[15]. We derived an upper bound on the interference probability, $\Pr(\rho_k = 1)$ as a function of the code family and the physical location of both the desired client and interferers. We also demonstrated that a uniform radial (UR) distribution for the clients, while simple and easy to model, provides an acceptable estimate, in terms of SIR, for more general geographical distribution models [7]. Therefore, in this paper we assume that client distribution over the network coverage area obeys a UR model.

C. Decoded Signal

By considering unitary cross-correlation, $\lambda_c = 1$ for codes used, each interfering CM sequence can only contribute one optical pulse to the total decoded signal in the observation interval. We assume that the CO receiver knows the exact observation interval T_{obs} (corresponding to the auto-correlation peak window)[1] for the desired CM_1 [7],[14]. The decoded signal for the desired customer in the field domain as a function of time t and wavelength λ during $t \in T_{obs}$ can be expressed as (see eq. (14) in [7]) in (1) where vector $\underline{l} = [l_1, ..., l_K]$ represents the distance from the clients to the CO. Other terms are defined in the following, per [7].

The first term in (1) is the desired signal, the auto-correlation peak. The second term corresponds to the interference coming from undesired clients, i.e., cross-correlation spikes. The total connector/splice loss is α_L, the transmission fiber loss is α_a in neper/meter in the monitoring wavelength[2], and the CM (decoding) attenuation in the field domain is α_{CM} (α_d); which are discussed in greater details at the end of this subsection. The decoded signal experiences attenuation proportional to the number of clients K due to splitting and

[1]The synchronization of the receiver to the observation interval is an important issue which is not in the purpose of this paper.

[2]U band fiber loss is higher than the data bands (C and L), see Table I.

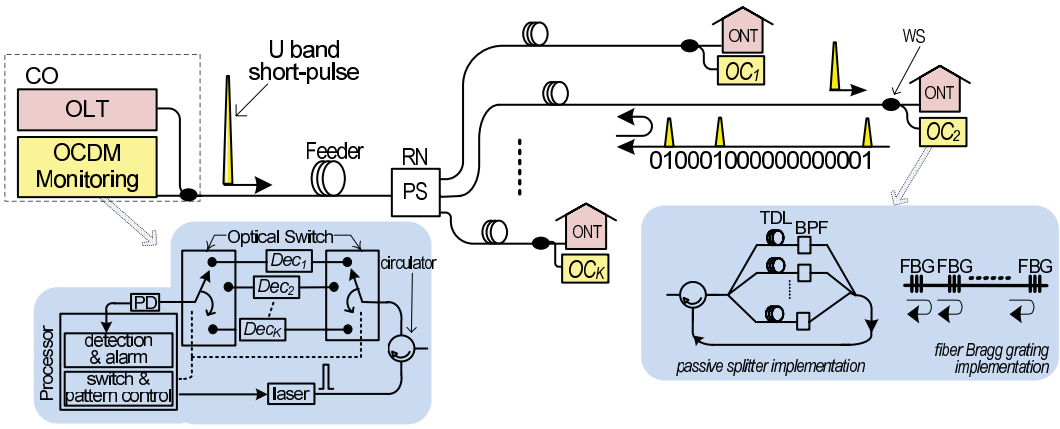

Fig. 1. Principle of OCDM based monitoring technique; the same implementation is considered for encoding/decoding operation.

$$r_1(t,\lambda,\underline{l}) = \frac{\sqrt{\alpha_L}\alpha_{CM}\alpha_d}{K}\left[\xi_1 e^{-\alpha_a l_1}\sum_{u=1}^{w}\Pi(t,\lambda_{1,u}) + \sum_{k=2}^{K}\rho_k e^{-\alpha_a l_k}\Pi(t,\upsilon_k)\right] \quad (1)$$

combining at the RN, i.e., a total power insertion loss of $\frac{1}{K^2}$. The binary random variable $\xi_1 \in \{0,1\}$ denotes the status of the desired client's connection. The frequency in common between user 1 and user k is denoted by υ_k, while $\lambda_{1,u}$ is the uth frequency in user 1's code. We will now consider the impact of our choice of system architecture on (1), both for 1D vs. 2D codes, and the encoder implementation. The source coherence effects, coherent (laser) or incoherent/broadband source (BBS), and coding schemes and their relation to noise sources are discussed in section III.

In a 1D scheme only one wavelength is transmitted, so all the pulses in (1) have the same center wavelength, i.e., $\lambda_{1,u} = \lambda_0$ and $\upsilon_k = \lambda_0$. However, in a 2D case, υ_k varies with the code and interfering client, hence reducing the total beat noise (BN) terms. In fact, due to the coding in the wavelength domain, a 2D scheme suffers less from BN than a 1D scheme, see section III. The encoding attenuation (α_e) depends on the implementation used for our OC monitoring system [6]-[7],[14],[15]. The PSC with TDL and optical BPFs has $\alpha_e^{\text{2D}} = \alpha_e^{\text{1D}} = \frac{1}{w}$. The additional circulator (with attenuation factor α_{circ}) increases the CM insertion loss, i.e., $\alpha_{CM} = \alpha_{circ}\alpha_e$. Typical values of 2-3dB are considered for the total power insertion loss of the circulator. For a FBG implementation of 1D coding we have $\alpha_{CM}^{\text{1D}} = \alpha_e^{\text{1D}} = \frac{1}{\sqrt{w}}$ where all the gratings are tuned to reflect the same wavelength. For a FBG implementation of 2D coding, we have $\alpha_{CM}^{\text{2D}} = \alpha_e^{\text{2D}} = \alpha_r$ where α_r is the reflectivity of the grating for 2D scheme [6],[7],[15],[16]. For a 2D scheme, each grating is designed to reflect a distinct wavelength with $\alpha_r = 100\%$ reflectivity. However, for a 1D scheme the reflectivities depend on the code weight w. As mentioned, the same implementation is considered for encoding and decoding operation, i.e., $\alpha_e = \alpha_d$.

D. Detected Signal

In this paper we use a square law model for the detection process, and include all electrical and optical noises as well [17]-[19]. Also, in order to compensate the huge loss due to passive elements such as splitter/combiner, we consider a high gain avalanche photodiode (APD) with a gain G and excess noise factor of $1+\zeta$, see Table I. Recall that no optical amplifier exists for the U band. The total output photocurrent can be written as

$$\begin{aligned} i_{PD}(t) \triangleq\ & G\left|r_1(t,\lambda,\underline{l})\right|^2 \\ & + i_{RIN}(t) + i_{SN}(t) + i_{DN}(t) + i_{TN}(t) \end{aligned} \quad (2)$$

for $t \in T_{obs}$. The terms $i_{RIN}(t)$, $i_{SN}(t)$, $i_{TN}(t)$ and $i_{DN}(t)$ denote current noise sources: relative intensity noise (RIN) of the detected optical pulses, shot noise (SN), dark current noise (DN), and thermal noise (TN) of the receiver. The first three terms in (2) are the sources of signal (and interference) dependent noises. The remaining terms in (2) correspond to the signal independent noises.

Consider traditional OTDR on point-to-point (PTP) links. In these systems the receiver sensitivity is limited by the shot noise, since the measurements can be taken over a very long interval. There is no RIN because coherent (laser) sources are used; there is no beat noise (BN) because only one optical pulse is transmitted and reflected by the network [19]. In contrast, in our application measurements cannot be taken over a long interval, but are restricted to the brief observation interval T_{obs} with duration of a transmitted pulse width. Incoherent sources offer advantages, but introduce RIN. Finally, due to the tree structure, as opposed to PTP, many pulses are returned leading to BN. In the next section we show that these differences affect our system performance analysis.

III. Noise Source Analysis

In subsection A, we address potential structures for our monitoring system. In subsection B we derive analytically the total detected light, including the source coherence effects, i.e., BN and RIN (SN, TN, and DN are in subsection C). We examine both coherent and broadband sources and 2D and 1D coding schemes. These equations are used later to study system performance.

A. Potential System Structures

Taking two possible source types (coherent and BBS), two coding schemes (1D and 2D), and two encoding/decoding implementations (FBG and PSC), a variety of architectures can be proposed for our monitoring system [7]. In fact, considering the power/loss budget, some combinations are extremely disadvantageous. For instance, due to the very poor performance of the coherent source based 1D coding scheme, a PSC based implementation of this scheme is not considered in this paper. In addition, the spectrum slicing of the BBS leads to intensity noise for a 2D coding scheme that is prohibitive, and thus this is not addressed. Recall that a filtered BBS severely suffers from RIN [19]. Therefore, we consider only the following four configurations to be of most interest: 1) coherent source + 1D FBG enc/dec (1D-Coh-FBG), 2) BBS + 1D FBG enc/dec (1D-BBS-FBG), 3) BBS + 1D PSC enc/dec (1D-BBS-PSC), and 4) coherent source + 2D FBG enc/dec (2D-Coh-FBG).

B. Beat Noise and DC Components

To develop equations for the beat noise contribution for either coherent or incoherent sources, we focus on the first term in (2) and decompose it. Let $i_{IA}(t)$ represent the intensity (power) addition and $i_{BN}(t)$ the beating of the detected pulses (desired and interferers), i.e., $G\left|r_1(t,\lambda,\underline{l})\right|^2 = i_{IA}(t) + i_{BN}(t)$. Recall that in [7] we assumed that the total output current can be approximated solely by the intensity addition term, i.e., $i_{PD}(t) = i_{IA}(t)$. Using (2) in conjugation with (1) we have equation (3) as expressed at the top of the page.

where by definition $\alpha_T \triangleq \frac{\alpha_L \alpha_{CM}^2 \alpha_d^2}{K^2}$ represents the total loss experienced by each optical pulse. Similar to (3) the BN term $i_{BN}(t)$ can be written as given by (4) at the top of the page. Where $Re\{x\} \triangleq \frac{x+x^*}{2}$ and $*$ denotes the complex conjugate. Three beating signals are defined: signal-to-signal beating (SSB), signal-to-interference beating (SIB), and interference-to-interference beating (IIB). The photocurrent $i_{PD}(t)$ will be electrically filtered, affecting the contributions to BN from terms SSB, SIB, and IIB. The beating between pulses with different center wavelengths is eliminated by electrical filtering; beating is significant only for signals with the same center wavelength. In case of the 1D scheme, and all terms in (4), i.e., SSB, SIB, and IIB, contribute to a significant BN power. However, for the 2D scheme, SSB is eliminated by assigning unique wavelengths to the pulses in the auto-correlation peak in (1), i.e., $\lambda_{1,u} \neq \lambda_{1,v}$ for $u \neq v \in \{1,...,w\}$. In addition, the average power of SIB and IIB decreases proportionally with the code weight w [20]-[25]. The total BN power also depends on the statistics of the interference $\{\rho_k\}_{k=2}^{K}$, particularly on the geographical distribution of the clients and the transmitted pulse width T_c. Rather than standard optical CDMA, decreasing T_c directly decreases the interference by reducing the correlation distance. In addition, sparser users leads to smaller interference probability $\Pr(\rho_k = 1)$ [7]. In this paper, we consider a fixed coverage area and a UR distribution for the customers, i.e., we only investigate the importance of T_c on our monitoring performance, for more details see [7].

To estimate the desired DDF status ξ_1 the photocurrent $i_{PD}(t)$ is electrically filtered during T_{obs} of length T_c, see

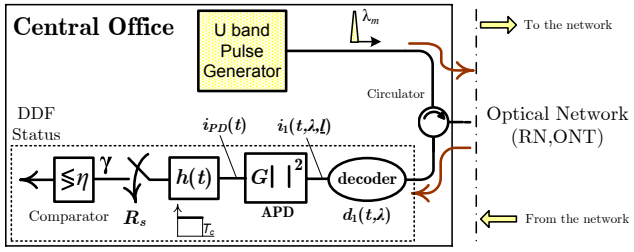

Fig. 2. Illustration of the CO structure: transmitter and receiver; the optical switches in Fig.1 are considered ideal with no insertion loss.

Fig. 2. The filtered signal is then sampled and the decision variable is compared to a threshold which depends on the system parameters, see section VI. In the case of an integrator for the electrical filter, the decision random variable can be written as

$$\gamma \triangleq \frac{1}{T_c} \int\limits_{t \in T_{obs}} i_{PD}(t)dt \tag{5}$$

The decision variable γ can be expressed as $\gamma = s_{IA} + \gamma_{BN} + \gamma_{RIN} + \gamma_{SN} + \gamma_{DN} + \gamma_{TN}$ where by definition we have $s_{IA} \triangleq \frac{1}{T_c} \int\limits_{t \in T_{obs}} i_{IA}(t)dt$ and $\gamma_j \triangleq \frac{1}{T_c} \int\limits_{t \in T_{obs}} i_j(t)dt$ for $j \in \{BN, RIN, SN, DN, TN\}$. Indeed γ_j are random variables representing the contribution of each noise component to γ, and s_{IA} denotes the non-zero average (DC) part of the filtered photocurrent. In our analysis we content ourselves with finding the signal power to noise power ratio, based on the second moments of γ_j; in section VI we study P_{FA} assuming Gaussian statistics for γ. To facilitate our analysis (in section VI) we keep explicit the desired DDF status ξ_1 in the following equations for both signal and noises.

The DC part s_{IA} can be written as the summation of the desired signal μ_{sig} and the interference contribution μ_{int}, i.e., $s_{IA} = \mu_{sig} + \mu_{int}$ where by definition

$$\begin{aligned}\mu_{sig}(l_1) &\triangleq \xi_1 G\alpha_T e^{-2\alpha_a l_1} \frac{1}{T_c} \sum_{u=1}^{w} \int_0^{T_c} \left|\Pi\left(t, \lambda_{1,u}\right)\right|^2 dt \\ &= \xi_1 w G\alpha_T P_s e^{-2\alpha_a l_1}\end{aligned} \tag{6}$$

$$\begin{aligned}\mu_{int}(\underline{l}) &\triangleq G\alpha_T \frac{1}{T_c} \sum_{k=2}^{K} \rho_k e^{-2\alpha_a l_k} \int_0^{T_c} \left|\Pi\left(t, \upsilon_k\right)\right|^2 dt \\ &= G\alpha_T P_s \sum_{k=2}^{K} \rho_k e^{-2\alpha_a l_k}\end{aligned} \tag{7}$$

We assumed that each pulse has average power $P_s = \frac{1}{T_c} \int_0^{T_c} \left|\Pi\left(t, \lambda\right)\right|^2 dt$. Note that μ_{sig} and μ_{int} are conditional means, i.e., conditioned on the realization of $\underline{l} = [l_1, ..., l_K]$. In the following we focus on the statistics of each of the noise terms γ_j contributing to γ (5).

C. Source Coherence Effects

In our proposed system the CO generates a pulse from a single source and transmits this to all CMs, introducing correlation in the reflected sequences. However, analysis in [26] shows that for relative delays larger than the observation interval, even optical pulses originating from the same source can be assumed independent at the output of the electrical

$$i_{IA}(t) \triangleq G\alpha_T \left[e^{-2\alpha_a l_1} \xi_1 \sum_{u=1}^{w} |\Pi(t,\lambda_{1,u})|^2 + \sum_{k=2}^{K} \rho_k e^{-2\alpha_a l_k} |\Pi(t,\upsilon_k)|^2 \right] \tag{3}$$

$$\begin{aligned} i_{BN}(t) \triangleq\ & \xi_1 G\alpha_T e^{-2\alpha_a l_1} \left(\sum_{i=1}^{w-1} \sum_{j=i+1}^{w} \underbrace{2\mathrm{Re}\left\{\Pi(t,\lambda_{1,i})\,\Pi^*(t,\lambda_{1,j})\right\}}_{\text{signal-to-signal beating} \triangleq \text{SSB}} \right) \\ & + \xi_1 G\alpha_T e^{-\alpha_a l_1} \left(\sum_{u=1}^{w} \sum_{k=2}^{K} \underbrace{2\rho_k e^{-\alpha_a l_k} Re\left\{\Pi(t,\lambda_{1,u})\,\Pi^*(t,\upsilon_k)\right\}}_{\text{signal-to-interference beating} \triangleq \text{SIB}} \right) \\ & + G\alpha_T \left(\sum_{i=2}^{K-1} \sum_{j=i+1}^{K} \underbrace{2\rho_i\rho_j e^{-\alpha_a(l_i+l_j)} Re\left\{\Pi(t,\upsilon_i)\,\Pi^*(t,\upsilon_j)\right\}}_{\text{interference-to-interference beating} \triangleq \text{IIB}} \right) \end{aligned} \tag{4}$$

filter. Recall that in our application the pulse width is small, especially compared to the geographic distribution of clients; in order for returns to remain correlated clients would need to be spaced closer than a meter. We therefore assume random variables γ_{RIN} and γ_{BN} are uncorrelated. By assuming a linear model in the field domain for all the network components as in [7] and neglecting polarization effects, the return signal is composed of delayed (and attenuated) versions of the original monitoring pulse sent by the CO. In sum, all incident pulses on the photodetector have identical but independent statistics so that all the beating terms in (4) are uncorrelated. The total noise power (conditioned on $\underline{l}$) due to the RIN (σ^2_{RIN}) and BN (σ^2_{BN}) can be simply summed in order to calculate the total RIN and BN power, i.e., $\sigma^2_{RIN} + \sigma^2_{BN}$ [17],[18],[19]. Again recall that RIN and BN powers are also affected by the transmitted pulse width and the geographical distribution of the users in the network, see Section V.

i) RIN for a BBS source in 1D scheme

Let β be the source coherence time of the optical signal divided by the pulse duration, i.e., $\beta = \frac{\tau_c}{T_c}$. The filtered RIN of such a signal has a normalized power equal to β [17],[19]. For electrical bandwidth B_e and available optical bandwidth B_o, we have $\beta \cong \frac{B_e}{B_o}$. Therefore, the RIN power of an optical signal, σ^2_{RIN}, is β times the square of its power. Using (3), the total RIN power can be expressed as

$$\begin{aligned} \sigma^2_{RIN}(\xi_1,\underline{l}) = {} & \beta(\alpha_T G P_s)^2(1+\zeta) \\ & \times \left[\xi_1 w e^{-4\alpha_a l_1} + \sum_{k=2}^{K} \rho_k e^{-4\alpha_a l_k} \right] \end{aligned} \tag{8}$$

Recall that in a laser based system no significant RIN exists, i.e., $\sigma_{RIN} = 0$. As mentioned, due to the spectrum slicing of the BBS source, a 2D scheme that uses BBS suffers from severe RIN [19]. Therefore, in our application we do not consider BBS sources for 2D coding schemes, but rather only coherent sources (lasers) for 2D.

ii) BN in a 1D Scheme (laser and BBS)

Similar to RIN, each beat noise term for both coherent and incoherent sources in (4) has a normalized power equal to β, where by definition $\beta = \min\left(\frac{\tau_c}{T_c} \cong \frac{B_e}{B_o}, 1\right)$ [17,19,21]. The optical bandwidth B_o however depends on the source type. For instance, a coherent source such as a mode-locked laser has B_o around 10 MHz. For a broadband source such as thermal sources or LEDs, B_o can be as large as 1THz ($\sim$ 8 nm). For pulse width larger than the source coherence time, i.e., $T_c \geq \tau_c$, β is proportional to the inverse of the pulse width for both coherent and BBS sources.

The optical signal for both lasers and BBS is assumed to have a zero mean average in the field domain. Thus all terms in (4) are uncorrelated and so correspondingly are SSB, SIB, and IIB uncorrelated. The total BN power can then be expressed as the summation of the power of each BN term component in (4). The BN power of each Re term in (4) is β times of the square of its power, as for RIN terms [17]-[19],[26]. Therefore, the conditional powers of SSB, SIB, and IIB are

$$\sigma^2_{BN}(\xi_1,\underline{l}) = \sigma^2_{SSB}(\xi_1,l_1) + \sigma^2_{SIB}(\xi_1,\underline{l}) + \sigma^2_{IIB}(\underline{l}) \tag{9}$$

where we have

$$\sigma^2_{SSB}(\xi_1,l_1) = \xi_1\beta(\alpha_T G P_s)^2(1+\zeta)w(w-1)e^{-4\alpha_a l_1} \tag{10}$$

$$\begin{aligned} \sigma^2_{SIB}(\xi_1,\underline{l}) = {} & \xi_1\beta(\alpha_T G P_s)^2(1+\zeta) \\ & \times w e^{-2\alpha_a l_1} \sum_{k=2}^{K} 2\rho_k e^{-2\alpha_a l_k} \end{aligned} \tag{11}$$

$$\begin{aligned} \sigma^2_{IIB}(\underline{l}) = {} & \beta(\alpha_T G P_s)^2(1+\zeta) \\ & \times \sum_{u=2}^{K-1} \sum_{v=u+1}^{K} 2\rho_u\rho_v e^{-2\alpha_a(l_u+l_v)} \end{aligned} \tag{12}$$

Note that (9) hold for both coherent and BBS in a 1D coding scheme. Also $\{\rho_k\}$ depend on the geographic distribution of clients and the transmitted pulse width [7].

iii) BN for a laser source in a 2D Schem

In a 2D scheme, by assigning a different wavelength to each pulse in the code, the autocorrelation will contain no BN among desired pulses, i.e., SSB is zero [15],[16],[21]-[25][3]. As mentioned previously, for 2D scheme, (9-2) and (9-3) reduces by a factor of w. The 2D scheme has a double benefit: eliminating SSB and reducing SIB and IIB. IIB is

[3]For this to be true the number of available wavelength should be higher than the code weight, i.e., $M \geq w$.

on average much smaller than SIB, so we can approximate $\sigma^2_{BN}(\xi_1, \underline{l}) \approx \sigma^2_{SIB}(\xi_1, \underline{l})$. As mentioned, due to the significant RIN power of a spectrum sliced BBS, in this paper we do not consider a 2D scheme that uses BBS sources.

D. Shot, Dark Current & Thermal Noises

The shot noise process, $i_{SN}(t)$, is modeled as a Poisson process with a power proportional to the average of the detected light in (3), and independent of all other noise components [17]-[19]. Therefore, the random variable γ_{SN} is Poisson with a conditional power equal to

$$\sigma^2_{SN} \triangleq qG(1+\zeta)s_{IA}B_e = qG(1+\zeta)(\mu_{sig}+\mu_{int})B_e \quad (13)$$

where q is the electron charge.

As with the shot noise process, the dark current noise is modeled by a Poisson process with an average current equal to I_{DN} Amps and is independent of all other noise components. The filtered dark current, γ_{DN} is a Poisson random variable with a power $\sigma^2_{DN} = qI_{DN}B_e$. Thermal noise is modeled as a zero mean Gaussian process with a power spectral density N_{TN} in Amp^2/Hz [17]-[19]. So the filtered thermal noise γ_{TN} is a zero mean Gaussian random variable with a power equal to $\sigma^2_{TN} = N_{TN}B_e$.

Based on previous discussion, all the noise components $\gamma_j, j \in \{BN, RIN, SN, DN, TN\}$ are uncorrelated. Therefore, the total noise power due to RIN, BN, SN, DN and TN can be simply calculated by adding all noise component powers. We define a new random variable γ_n representing the total noise effect in (5) so as $\gamma_n \triangleq \gamma_{BN} + \gamma_{RIN} + \gamma_{SN} + \gamma_{DN} + \gamma_{TN}$. The random variable γ_n is zero mean and its conditional (conditioned on realization $\underline{l}$) power σ^2_n equals to $\sigma^2_n = \sigma^2_{BN} + \sigma^2_{RIN} + \sigma^2_{SN} + \sigma^2_{DN} + \sigma^2_{TN}$. Usually γ_n is approximated to be Gaussian [17]-[19], see section VI[27].

IV. Performance Evaluation

Due to non-zero interference coming from undesired clients in the network, three signal quality measurement tools can be defined: signal-to-interference ratio (SIR), signal-to-noise ratio (SNR), and signal-to-noise-plus-interference ratio (SNIR). We can express SNIR in terms of SNR and SIR (previously studied in [7]).

A. Signal Quality Measurment Tools

By definition SNIR is the square of the desired signal average (auto-correlation peak) divided by the average of the total noise power

$$SNIR \triangleq \frac{\overline{\mu}^2_{sig}}{\overline{\mu}^2_{int} + \overline{\sigma^2_n}} \quad (14)$$

where $\overline{\mu}_{sig} = E\{\mu_{sig}\}$, $\overline{\mu}_{int} = E\{\mu_{int}\}$ and $\overline{\sigma^2_n} = E\{\sigma^2_n\}$ is the average of desired signal, interference, and noises; the operator $E\{\cdot\}$ takes the expectation over $\underline{l}$ and ξ_1. The a priori probability of a fault in the desired client's DDF is $p_\xi = \Pr(\xi_1 = 0)$. As the link is reasonably reliable, $E\{\xi_1\} = 1 - p_\xi \cong 1$. The denominator in (14) corresponds to the total power of undesired terms, including undesired DC in (5). The signal-to-noise ratio (SNR) is defined as

$$SNR \triangleq \frac{\overline{\mu}^2_{sig}}{\overline{\sigma^2_n}} \quad (15)$$

Using the signal-to-interference ratio (SIR) definition in [7], i.e., $\sqrt{SIR} \triangleq \frac{\overline{\mu}_{sig}}{\overline{\mu}_{int}}$, SNIR and SNR are related by

$$SNIR^{-1} = SIR^{-1} + SNR^{-1} \quad (16)$$

So having SIR and SNR gives us SNIR using (16). We continue our discussion by defining measurement tools to focus on each noise term separately. By dividing both the numerator and denominator of (15) by $\overline{\mu}^2_{sig}$ we define the SNR component $SNR_i \triangleq \frac{\overline{\mu^2_{sig}}}{\overline{\sigma^2_i}}$ for $i \in \{BN, RIN, SN, DN, TN\}$ where by definition $\overline{\sigma^2_i} \triangleq E\{\sigma^2_i\}$. Therefore, we can write $SNR^{-1} = \sum_i SNR_i^{-1}$. In the following, we will see that, depending on the coding schemes and encoding/decoding implementations and network parameters, different SNIR components become dominant.

In the following we evaluate the importance of transmitted power, network size, and the DDF fault probability on our system performance. The averages of the signal and noise powers in (8)-(13) are calculated by performing expectation over all possible network realizations $\underline{l} = [l_1, ..., l_K]$. We assume that the client distribution obeys a uniform radial (UR) model introduced in [7]. As explained before, a fixed coverage area equal to 1 km^2 is considered. This corresponds to a maximum separation length of $\Delta l = 564$ m for a UR distribution model[4]. Table I gives the parameters we used for our numerical results. While BBS pulses suffer from severe dispersion, for this paper we assume perfect dispersion compensation at the CO.

B. Transmitted Power

Consider a PON with $K = 64$ clients and a 20 km feeder fiber. The total loss due to splitting/combining at the RN is 36 dB (18 dB +18 dB). The total feeder loss is 12 dB (6 dB+6 dB). For a code weight of $w = 4$, the total encoder/decoder insertion loss is 12 dB for 1D FBG, 0 dB for 2D FBG, 26 dB for a PSC based implementation. Therefore, for a 5 dB splice/connector loss, the total loss experienced by optical pulses varies from 53 dB to 79 dB. Considering a transmitted power of 4 dBm, the received power can be as small as -49 dBm (2D FBG) to -75 dBm (PSC). In the next, we investigate the importance of transmitted power on the performance of our monitoring system.

Using Table I, the required code length is $F = 769$. For a $T_c = 1$ ns pulse width we have $l_{CD} = 76.9$ m. In this case, we have SIRs of 21.6 dB for 1D coding scheme and 33.6 dB for 2D coding scheme; the system is interference-free [7]. In Fig. 3 we plot SNIR (solid line) and SNR (dashed line) versus the transmitted power for different configurations. Only transmitted powers up to 10 dBm are considered, as maximum power is limited by the fiber nonlinearity; for

[4]The maximum distance between the RN and a customer in the network (CM) [7].

TABLE I
VALUES USED FOR SIMULATION.

Geographical Parameters	
Feeder Length	$l_f = 20$ km
Coverage Area	$a^2 = 1$ km^2
Maximum Separation Length	$\Delta l = 564$ m
Fiber Fault Probability	$p_\xi = 10^{-2}$
Geographical Distribution	Uniform Radial over $[0, \Delta l]$
MW-OOC Parameters	
Number of Wavelengths	$M = 4$
Code Weight	$w = 4$
Maximum of Auto-correlation	$\lambda_a = 1$
Maximum of Cross-correlation	$\lambda_c = 1$
Code Length (varies with K)	$F = w(w-1)K + 1$
Component Parameters	
Monitoring Wavelength	$\lambda_m = 1650$ nm
Fiber Attenuation for λ_m	$\alpha = 0.3$ dB/km
Avalanch Photodiode (APD) Gain	$G = 100$
APD Ionization Coefficient	$\chi = 10^{-2}$
APD Excess Noise Factor	$\zeta + 1 = 2.97$
Dark Current	$I_{DC} = 160$ nA
Thermal Noise Power	$N_{TN} = 10^{-26}$ Amp^2/Hz
Total Connector/Splice Loss	$\alpha_L = 5$ dB
BBS Bandwidth	B_o =1 THz and 100 GHz
Laser Linewidth	B_o =10 MHz
β (varies with pulse width T_c)	$B_e/B_o = 1/(B_o T_c)$
Splitter/Network Size at RN	$K = 8, 16, 32, 64, 128, 256$

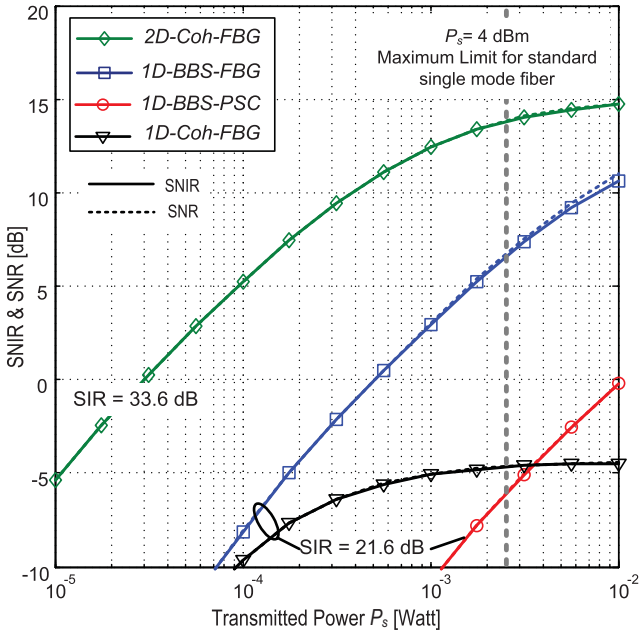

Fig. 3. SNIR (solid curve) and SNR (dashed curve) versus the transmitted pulse power for pulse width $T_c = 1$ ns and $K = 64$; $B_o = 1$ THz for a BBS source and $B_o = 10$ MHz for a coherent source.

higher values, the linear system assumption is no longer valid [7]. We observe negligible difference between SNIR and SNR. Performance is limited by detection noise and not the interference. From Fig. 3 we observe that only 2D-Coh-FBG provides acceptable performance, i.e., SNIR $\sim$10 dB, for powers smaller than 4 dBm. In the rest of the paper, we consider 4 dBm for the transmitted power which is the maximum possible value for a standard single mode fiber in order not to induce any fiber nonlinearity [19].

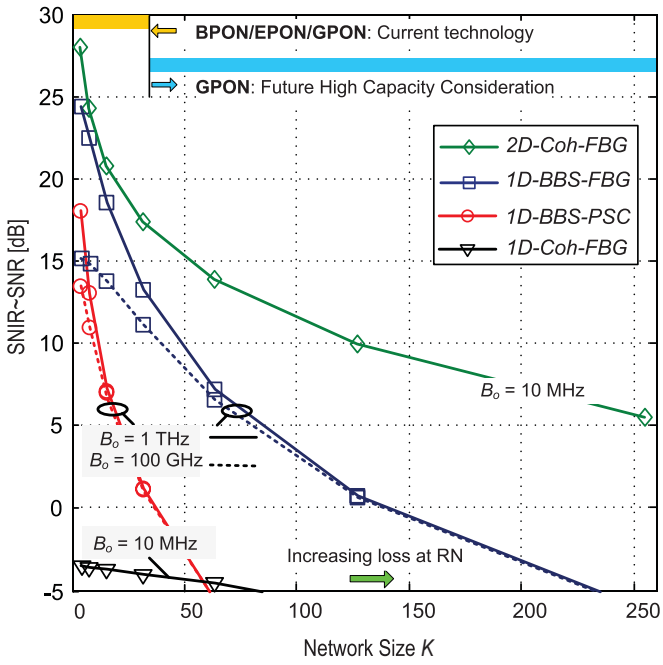

Fig. 4. SNR versus network size for different coding schemes and $P_s = 4$ dBm and $T_c = 1$ ns.

C. Network Size and Fault Probability

Using $T_c = 1$ ns, $P_s = 4$ dBm and values in Table I, in Fig. 4 we plot the SNIR ($\cong$ SNR) versus network size for both 1D and 2D schemes. It can be observed that for a 1D scheme that uses coherent sources, the performance is very poor even for small network sizes, see section III. Increasing the network capacity degrades SNIR and SNR (as well as SIR [7]) by increasing the splitting loss at the RN (as well as the interference). We also considered (perfectly compensated) BBS sources with $B_o = 1$ THz (solid line) and $B_o = 100$ GHz (dashed line) for a 1D scheme and different coding implementation in Fig. 4. Increasing B_o leads to considerable improvement in system performance, see (8)-(12). Fig. 4 shows that even for small network sizes such as $K = 32$, the performance of both 1D-Coh-FBG and 1D-BBS-PSC are poor, i.e., SNIR $\leq$ 5dB. Having established form Fig. 3 and Fig. 4 that the 1D-Coh-FBG and 1D-BBS-PSC are not viable solutions, we retain only the 1D-BBS-FBG and 2D-Coh-FBG structures as candidates for our monitoring system.

Regions corresponding to the current PON technology (E/B/GPON) and future high capacity PON (GPON with $K = 64, 128, 256$) are also illustrated [5,6,7]. We see our technique, while supporting the current standards, enables further increases in the splitting ratio at the RN. Recall that all the results presented in Fig.4 are related to the parameters listed in Table I.

The a priori probability of a fault in the desired client's DDF is $p_\xi = \Pr(\xi_1 = 0)$. As the link is reasonably reliable, $E\{\xi_1\} = 1 - p_\xi \approx 1$. This approximation leads to insignificant variation in system SNIR ($\sim$SNR) versus network size; for instance, plots are nearly indistinguishable for $p_\xi = 10^{-2}$ versus $p_\xi = 10^{-1}$ for $T_c = 1$ ns, $P_s = 4$ dBm and the values in Table I.

V. Effect of Pulse Width

In this section we focus on the effect of pulse width on our monitoring system performance in terms of SNIR. While an interference limited analysis shows that decreasing pulse width increases SIR unboundedly [7], we show that, as a result of trade-off between interference and detection noises (BN, RIN and SN) the pulse width can be optimized depending on the network size and coding implementations. As explained before, we only focus on 1D-BBS-FBG and 2D-Coh-FBG architectures. In all the results presented here, the bandwidth of the photodetector is considered to be greater than the post-detection electrical bandwidth, i.e., larger than $\frac{1}{T_c}$. Therefore, our numerical results do not take the bandwidth limitation of the photodetector into consideration.

A. Numerical Results

Using the values in Table I and $P_s = 4$ dBm, in Fig. 5a we plot the SNIR given by (14) versus the pulse width for a 1D-BBS-FBG system and different network sizes. For short pulse width, or equivalently high electrical bandwidths, (left side of Fig. 5a) the performance is limited by the signal dependent noises. As the pulse width increases, SNR improves while SIR degrades[5]. For longer pulses (when $l_{CD} = cFT_c/2 \geq \Delta l$), the SNIR is dominated by SIR. For very long pulse widths our system tends to SIR=10 dB; in this regime we have a high density PON whose performance is similar to that of a data bearing OCDMA system [7]. Fig. 5a also shows that for small networks, $K = 8, 16, 32$ an optimal pulse width exists which provides the maximum SNIR. This optimal pulse width occurs at $T_c \approx 1$ ns in our simulations based on the values given in Table I. For large network sizes ($K = 64, 128, 256$) no optimal pulse width is observed and all very long pulses lead to the same asymptotic performance studied in [7].

Using the values in Table I and $P_s = 4$ dBm, we plot SNIR in (14) versus the pulse width for a 2D-Coh-FBG system architecture and different network sizes in Fig. 5b. For very short pulses it is more likely that $l_{CD} \ll \Delta l$, i.e., negligible interference; SIR is high, and SIB power can be neglected compared to the shot noise power. Thus the total noise power for short pulses is dominated by the shot noise coming from the desired pulses, i.e., SNIR $\approx$ SNR$_{SN}$, a linearly increasing function of the pulse width. As the pulse width increases, leading to higher correlation distance l_{CD}, interference increases leading to greater beat noise power [7]. For these intermediate pulse widths, beat noise dominates, SNIR $\approx$ SNR$_{BN}$, and we observe the SNIR (in dB) is a linearly decreasing function of pulse width. When l_{CD} reaches $\Delta l = cFT_c/2$, the interference reaches a maximum (thus fixing SIR and SNR$_{BN}$) after which the SNIR plateaus. Once the pulse width exceeds the coherence time of the laser source ($T_c \geq \tau_c$), SNR$_{BN}$ improves. Thus for very long pulse widths the system is interference limited (high density PON) with SNIR $\approx$ SIR $= 22$ dB.

Compared to a 1D scheme, for network sizes up to $K = 128$, a shorter locally optimal pulse width exists, $T_c \approx 0.3$ ns. As was the case in the 1D scheme, for $K > 64$ the highest SNIR is achieved asymptotically with very long pulse widths. The optimal pulse width exists as very short pulse widths give good SIR, but low SNR. Correspondingly, for long pulse widths SIR degrades while SNR improves. In subsection C we provide analytical expressions for this optimal value depending on the network parameters.

[5]In [7] we found that SIR (in dB) is a linearly decreasing function of the pulse width for $l_{CD} = cFT_c/2 \leq \Delta l$.

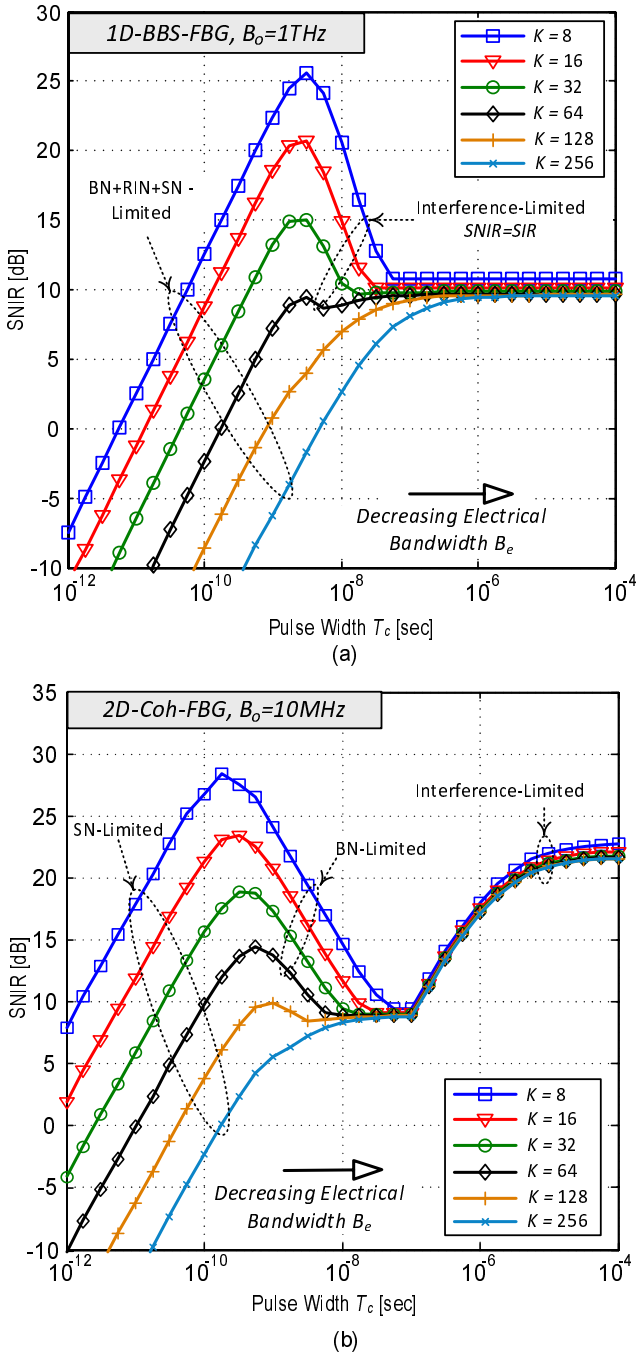

Fig. 5. SNIR versus the transmitted pulse width for $P_s = 4$ dBm and a) 2D-Coh-FBG with $B_o = 10$ MHz, and b) 1D-BBS-FBG and $B_o = 1$ THz.

B. Partitioning of Monitoring Across U-band Sub-bands

As illustrated in Fig. 5, for large networks, particularly for the 2D scheme, the optimal performance is only achieved for very long pulse widths. For smaller networks, the local

maximums in Fig. 5 are opportunities to increase the effectiveness of our monitoring system. In addition, these network sizes lead to optimal pulse widths with easier encoder/decoder implementations. For instance, for a very short pulse, the encoder/decoder will have greater sensitivity; also, very long pulses this will be bulky to the point of impracticality.

Recall that all 50 nm in the U band (1625-1675 nm) is devoted to monitoring and no data is carried inside this band. In order to achieve good performance and practical monitoring and still support large networks, we propose the use of a multiband scheme for the monitoring. For example, in the case of a 1D scheme that uses BBS we can slice the 50 nm of U band into five slices of 8 nm ($B_o = 1$ THz) and leave the remaining 10 nm for a guard band. The monitoring capacity is then increased by a factor of five (the number of sub-bands) for the same SNIR (SNR) in Fig. 4. As a result similar to standard OTDR techniques averaging technique can be used to improve our system performance [19]. Assuming independent measurements, the SNR of the monitoring system improves in proportion to the number of measurements averaged.

In general, the partitioning and averaging techniques can be used simultaneously to significantly improve the performance/capacity of our monitoring system. The performance of our monitoring system is ultimately dominated by the interference, i.e., SNIR$\leq$SIR. In this situation the performance is only affected by the code properties, the geographic distribution and the transmitted pulse width [7].

C. Finding the Optimal Pulse Widths

We will assume that the transmitted power is high enough to neglect both the dark current and thermal noises, i.e., SNR_{DN}, $\text{SNR}_{TN} \to \infty$. Therefore, only signal dependent noises (BN, RIN and SN) are retained. We study 1D and 2D schemes separately. For space considerations only results are presented.

1D Coding Scheme

i) Short Pulses: As explained earlier, for sufficiently short pulses, SIR is very small and SNIR is dominated by other signal dependent noises. Thus the SNIR can be expressed as

$$SNIR = \frac{1}{B_o^{-1} + \Gamma} \frac{T_c}{1+\zeta} \qquad \begin{matrix}\text{for sufficiently} \\ \text{small } T_c\end{matrix} \tag{17}$$

where by definition $\Gamma^{-1} \triangleq w\alpha_T e^{-2\alpha_a l_f} P_s/q$. This equation validates our observation in Fig. 5 that for sufficiently short pulses, SNIR is a linear increasing function of pulse width.

ii) Long Pulses: For sufficiently long pulses, as observed in Fig. 5a, SNIR is dominated by interference, i.e., SNIR $\approx$ SIR. Note this is the region where an optimal pulse width exists, and SNIR is maximized. Recall $l_{CD} = cFT_c/2$ and $M = 1$ for 1D coding. Then from [7] eq. (22) we have

$$SNIR \cong SIR = \left((w-1)\frac{\Delta l}{cF}\right)^2 \frac{1}{T_c^2} \qquad \begin{matrix}\text{for sufficiently} \\ \text{large } T_c\end{matrix} \tag{18}$$

In this region SNIR is a decreasing function of T_c. The optimal pulse width and the corresponding SNIR can be approximated by the intersection of (17) and (18) as follows.

$$\begin{aligned} T_c^{opt} &= \left(\left(\tfrac{\Delta l}{cwK}\right)^2 (1+\zeta)\left(B_o^{-1}+\Gamma\right)\right)^{\frac{1}{3}} \\ &\to SNIR_{\max} = \tfrac{1}{2}\tfrac{1}{B_o^{-1}+\Gamma}\tfrac{T_c^{opt}}{1+\zeta} \end{aligned} \tag{19}$$

For instance, for a 1D scheme with $K = 16$ that uses a BBS with $B_o = 1$ THz, other parameters as given in Table I, yields $T_c^{opt} = 1.4$ ns and $\text{SNIR}_{\max} = 20.2$ dB. Comparing to results in Fig. 5a, we see these equations give good estimates.

2D Coding Scheme

i) Short Pulses: as discussed in subsection A, for sufficiently short pulses we have SNIR $\approx \text{SNR}_{SN}$. So

$$SNIR = \frac{T_c}{\Gamma(1+\zeta)} \qquad \begin{matrix}\text{for sufficiently} \\ \text{small } T_c\end{matrix} \tag{20}$$

where Γ is as defined previously. As observed in (20), we see a linear dependence on the transmitted pulse width.

ii) Long Pulses: As discussed previously, for longer pulses the performance is limited by BN, i.e., SNIR $\approx \text{SNR}_{BN}$. In this case we have;

$$SNIR = \left(\frac{M\Delta l}{2cK(1+\zeta)}\right)\frac{1}{T_c} \qquad \begin{matrix}\text{for longer} \\ T_c\end{matrix} \tag{21}$$

As in the 1D scheme, optimum pulse width and corresponding SNIR can be approximated from (20) and (21) as

$$T_c^{opt} = \sqrt{\frac{1}{2}\Gamma M\frac{\Delta l}{cK}} \to SNIR_{\max} = \frac{e^{-2\alpha_a l_f}\alpha_T w P_s}{2q(1+\zeta)} T_c^{opt} \tag{22}$$

As an example, for $K = 16$ and values in Table I for a 2D scheme, we have $T_c^{opt} = 0.38$ ns and $SNIR_{\max} = 24.4$ dB.

VI. False-Alarm and Detection Probabilities

Any CO error in the estimation of a desired DDF status, results in non-negligible operational expenditure (OPEX). Declaring a fiber fault when none exists results in an expensive and unnecessary truck-roll of complex fiber optic equipment. Alternately the CO failure to detect a fault in a DDF due to noisy measurement leads to customer dissatisfaction and complaints. Our monitoring system is similar to a multi-target radar system where both the detection (P_D) and false-alarm (P_{FA}) probabilities are of great importance, as in the OPEX application. These probabilities are inherently interdependent; it is easy to always have perfect detection if we always declare a fault, but our false-alarm probability would be abysmal. Therefore we employ Neyman-Pearson testing to maximize P_D subject to a limit on the false alarm probability P_{FA}. To visualize the trade-off between P_{FA} and P_D we use receiver operating characteristics (ROCs), that is a plot of achievable P_{FA} vs. P_D for a given SNR level [28]. In the following we study the ROCs of our monitoring technology for both 1D and 2D coding schemes and different network sizes.

By definition P_D is the probability of correctly declaring a DDF faulty, i.e., $P_D = \Pr(\gamma(\xi_1 = 0) \leq \eta)$ where η is the threshold of the comparator in Fig. 2. Similarly P_{FA} is the probability of declaring a DDF faulty when it is healthy, i.e., $P_{FA} = \Pr(\gamma(\xi_1 = 1) \leq \eta)$. Due to the contribution of different dependent/independent noises in the decision random variable in (5), the general derivation of P_{FA} and P_D is quite complex. In this paper, the distribution of γ is assumed to be Gaussian [14,21,27]. By assuming a Gaussian distribution for γ with conditional mean s_{IA} and power σ_n^2 and the definition of $Q(x) \triangleq \frac{1}{\sqrt{2\pi}}\int_x^\infty e^{-y^2/2}dy$, P_D and P_{FA} are related by $P_D = 1 - Q(\kappa Q^{-1}(1-P_{FA}) + \vartheta)$ where $\kappa \triangleq$

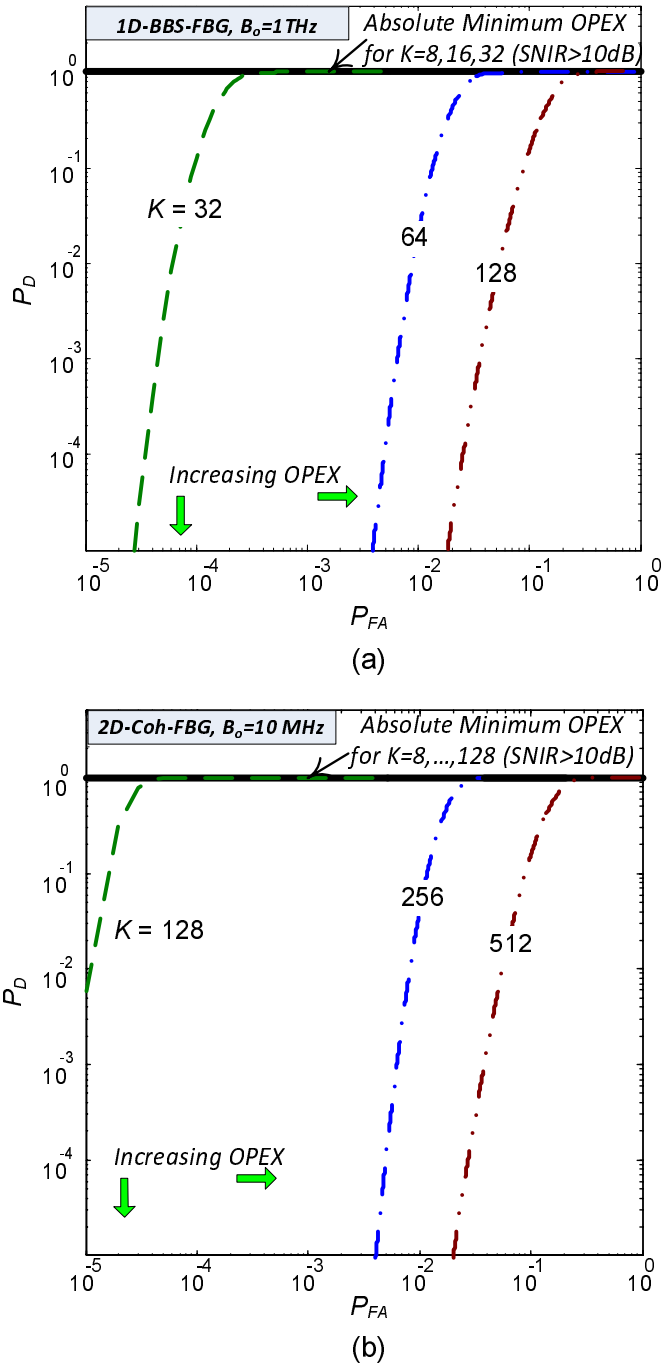

Fig. 6. ROC of the receiver for different system architectures and $P_s = 4$ dBm, $T_c = 1$ ns for a) 1D-BBS-FBG with $B_o = 1$ THz and b) 2D-Coh-FBG with $B_o = 10$ MHz.

$\overline{\sigma}_n(\xi_1 = 1)/\overline{\sigma}_n(\xi_1 = 0)$ and $\vartheta \triangleq \overline{\mu}_{sig}(\xi_1 = 1)/\overline{\sigma}_n(\xi_1 = 0)$. Fixing the threshold fixes both P_D and P_{FA}, i.e., each point in the ROC curve corresponds to a specific choice of the threshold of the comparator in Fig.2. The probability of failure to detect a fault is $1 - P_D$.

Using the values in Table I, $P_s = 4$ dBm and $T_c = 1$ ns the ROC for configurations 1D-BBS-FBG ($B_o = 1$ THz) and 2D-Coh-FBG ($B_o = 10$ MHz) are presented in Fig. 6. No averaging or partitioning is used for the results presented in Fig. 6. For a 1D-BBS-FBG system (Fig. 6a), ROC are flat for small network size, i.e., 8, 16, and 32. For instance, in a $K = 32$ customer network, when requiring a small P_{FA} (such as $P_{FA} = 10^{-3}$) P_D remains high ($P_D = 1$). As the network size increases, leading to smaller SNR, the ROC deteriorates. For $K = 64$ and the same P_{FA}, detection probability reduces to $P_D = 0$, i.e., high OPEX.

In Fig. 6b we plot ROC for a 2D-Coh-FBG system with $B_o = 10$ MHz. The ROC are considerably flat even for large network sizes. For a $K = 128$ customer network for small $P_{FA} = 10^{-3}$, the detection probability remains high, i.e., $P_D = 1$. Increasing the network size to $K = 256$ while keeping the same P_{FA} reduces detection probability to $P_D = 0$, i.e., high OPEX. As illustrated in Fig. 6, both 1D-BBS-FBG and 2D-Coh-FBG enables support of respectively 32 and 128 customers with negligible operational expenditure. SNIR$\geq$10 dB is required for optimal performance.

VII. Conclusion

In this paper, we analyzed the performance of an OCDM-based monitoring technique that offers a promising solution for fiber fault monitoring of future high capacity PON. We extended our analysis in [7] by using an accurate model for our monitoring system that includes both the interference and detection noises and realistic device parameters for our monitoring technology. We considered the nonlinear photo-detection process, including source coherence effects such as relative intensity noise (RIN) and beat noise (BN). Using the mathematics developed in this paper, and in conjunction with [7] where only signal-to-interference ratio (SIR) was treated, we addressed the importance of transmitted pulse power, pulse width, network size, fault probability as well as the source types (coherent or broadband) and coding schemes on our monitoring system performance. Our figures of merit for performance were signal-to-noise-plus-interference ratio (SNIR) and signal-to-noise ratio (SNR). We also investigated the receiver performance characteristics via Neyman-Pearson hypothesis testing. We showed optimal configurations for low operational expenditures.

Our analysis shows that two coding schemes stand out as the most promising: the one dimensional system using FBGs to slice an incoherent BBS source (1D-BBS-FBG), and a coherent source used with a two dimensional (time-wavelength) code implemented in FBGs (2D-Coh-FBG). We saw a performance advantage for the coherent solution in the 2D coding scheme. Our optical coding technique can support monitoring of a 128 client network with high SNIR, i.e., SNIR $\geq$10dB. As expected, the 2D scheme was shown to have better performance than the 1D approach. The capacity and performance of our monitoring system can be further improved by partitioning/averaging techniques, as explained. An experimental verification would be useful to explore the practicality of optical coding as a serious solution for the monitoring of future PON.

References

[1] A. Girard, “FTTx PON Technology and Testing," EXFO Electro-Optical Engineering Inc., Canada, 2005, ISBN: 1-55342-006-3.

[2] R. Davey, and D. Payne, “The future of optical transmission in access and metro networks-An operator’s point of view," *European Conf. Optical Commun. (ECOC)*, We 2.1.3, 2005.

[3] F. Caviglia and V. C. Biase, "Optical maintenance in PONs," *European Conf. Optical Commun. (ECOC)* , Madrid, Spain, pp. 621-625, 1998.
[4] D. C. Kilper, R. Bach, D. J. Blumenthal, D. Einstein, T. Landolsi, L. Ostar, M. Preiss, and A. E. Willner, "Optical performance monitoring," *IEEE J. Lightwave Technol.*, vol. 22, no. 1, pp. 294-304, Jan. 2004.
[5] M. D. Vaughn, D. Kozichek, D. Meis, A. Boskovic, and R. Wanger, "Value of reach-and-split ratio increase in FTTH access networks," *IEEE J. Lightwave Technol.*, vol. 22, no. 11, pp. 2617-2622, Nov. 2004.
[6] H. Fathallah and L. A. Rusch, "Code division multiplexing for in-service out-of-band monitoring," *J. Optical Netw.*, vol. 6, no. 7, pp. 819-829, July 2007.
[7] M. M. Rad, H. Fathallah, and L. A. Rusch, "Fiber fault PON monitoring using optical coding: effects of customer geographic distribution," *IEEE Trans. Commun.*, vol. 58, no. 4, Apr. 2010.
[8] S. Hann, J. Yoo, and C. Park, "Monitoring technique for a hybrid PS/WDM-PON by using a tunable OTDR and FBGs," *Meas. Sci. Technol.*, vol. 17, pp. 1070-1074, 2006.
[9] C. Yeh and S. Chi, "Optical fiber-fault surveillance for passive optical networks in S-band operation window," *Optics Express*, vol. 13, no. 14, pp. 5494-5498, July 2005.
[10] C. Chan, F. Tong, L. Chen, K. Ho, and D. Lam, "Fiber-fault identification for branched access networks using a wavelength-sweeping monitoring source," *IEEE Photonic Technol. Lett.*, vol. 11, no. 5, pp. 614-616, May 1999.
[11] N. Nakao, H. Izumita, T. Inoue, Y. Enomoto, N. Araki, and N. Tomito, "Maintenance method using 1650-nm wave-length band for optical fiber cable networks," *IEEE J. Lightwave Technol.*, vol. 19, no. 10, pp. 1513-1520, Oct. 2001.
[12] K. W. Lim, E. S. Son, K. H. Han, and Y. C. Chung, "Fault localization in WDM passive optical network by reusing downstream light source," *IEEE Photonic Technol. Lett.*, vol. 17, no. 12, pp. 2691-2693, Dec. 2005.
[13] S. B. Park, D. K. Jung, H. S. Shin, D. J. Shin, S. Hwang, Y. Oh, and C. Shim, "Optical fault monitoring method using broadband light source in WDM-PON," *IEE Electron. Lett.*, vol. 42, no. 4, Feb. 2006.
[14] G. Yang and W. C. Kwong, *Prime Codes with Applications to CDMA Optical and Wireless Networks*. Artech House, 2004 (ISBN: 1-58053-073-7).
[15] P. R. Prucnal, *Optical Code Division Multiple Access*. CRC Press, 2006 (ISBN: 0-8493-3683-X).
[16] H. Fathallah, L. A. Rusch, and S. LaRochelleh, "Passive optical fast frequency-hop CDMA communication system," *IEEE J. Lightwave Technol.*, vol. 17, no. 3, pp. 397-405, Mar. 1999.
[17] J. W. Goodman, *Statistical Optics*. John Wiley & Sons, 2000 (ISBN: 0-471-01502-4).
[18] R. M. Gagliardi and S. Karp, *Optical Communication*, Second Edition. John Wiley & Sons, 1995 (ISBN: 0-471-54287-3).
[19] D. Derickson, *Fiber Optic Test and Measurement*. Prentice Hall, 1998 (ISBN: 0-13-534330-5).
[20] L. Tancevski and L. A. Rusch, "Impact of beat noise on the performance of 2-D optical CDMA systems," *IEEE Commun. Lett.*, vol. 4, no. 8, pp. 264-266, Aug. 2000.
[21] T. M. Bazan, D. Harle, and I. Andonovic, "Mitigation of beat noise in time-wavelength optical code-division multiple-access," *IEEE J. Lightwave Technol.*, vol. 24, no. 11, pp. 4215-4222, Dec. 2006.
[22] X. Wang and K. Kitayama, "Analysis of beat noise in coherent and incoherent time spreading OCDMA," *IEEE J. Lightwave Technol.*, vol. 22, pp. 2226-2235, Oct. 2004.
[23] T. Bazan, D. Harle, I. Andonovic, and M. Meenakshi, "The effect of beat noise on the performance of 2D time/spreading wavelength hopping optical CDMA systems," *J. Optical Netwo.*, vol. 4, pp. 121-129, Mar. 2005.
[24] S. Ayott and L. A. Rusch, "Experimental comparison of coherent versus incoherent sources in four-user $\lambda - t$ OCDMA system at 1.25 Gb/s," *IEEE Photonic Technol. Lett.*, vol. 17, pp. 2493-2495, Nov. 2005.
[25] C. Bres, Y. Huang, D. Rand, I. Glesk, P. R. Prucnal, T. Bazan, C. Michie, D. Harle, and I. Andpnovic, "On the experimental characterization of beat noise in 2D time-spreading wavelength hopping OCDMA systems," *IEEE Photonic Technol. Lett.*, vol. 18, no. 21, pp. 2314-2316, Nov. 2006.
[26] M. M. Rad and J. A. Salehi, "Phase-induced intensity noise in incoherent digital all-optical tapped-delay lines systems," *IEEE J. Lightwave Technol.*, vol. 24, no. 8, pp. 3059-3072, Aug. 2006.
[27] A. Papoulis and S. U. Pillai, *Probability, Random Variables and Stochastic Processes*, Fourth Edition. McGraw Hill, 2002 (ISBN: 0-07-366011-6).
[28] V. H. Trees, *An Introduction to Signal Detection and Estimation*. Springer, 1998 (ISBN: 0-387-94173-8).

Mohammad M. Rad received his B.S.E.E. and M.S.C. both from Sharif University of Technology in 2003 and 2005, respectively. In September 2006 he joined the Department of Electrical and Computer Engineering, Center for Optics, Photonics and Lasers (COPL), Université Laval as a PhD candidate. His research interests include fiber-optic communications, long haul data transmission, multiple access networks, network monitoring and sensor networks.

Habib A. Fathallah (S'96, M'01) received the B.S.E.E degree (with Honors) from the National Engineering School of Tunis, 1994 and the M.A. and Ph.D. degrees in electrical engineering from Laval University, Qc, Canada, in 1997 and 2001, respectively. He initiated the use of Bragg gratings technology for all-optical/all-fiber coding/decoding in Optical CDMA systems. He was the founder of Access Photonic Networks (2001- 2006). He is currently with Electrical Engineering Department, College of Engineering of the King Saud University (Riyadh, KSA) and adjunct professor with the Electrical and Computer Engineering Department of Laval University (Quebec, Canada). His research interests include optical communications systems and technologies, metro and access networks, Optical CDMA, PONs and long reach PONs, FTTH, Network Monitoring, and hybrid fiber wireless (FiWi) systems.

Leslie Ann Rusch (S'91-M'94-SM'00) L. A. Rusch received the B.S.E.E. (honors) degree from the California Institute of Technology, Pasadena, in 1980 and the M.A. and Ph.D. degrees in electrical engineering from Princeton University in 1992 and 1994, respectively. In 1994 she joined the Department of Electrical and Computer Engineering at Université Laval, Québec, QC, Canada, where she is currently a Full Professor performing research in wireless and optical communications. She managed a group researching new wireless technologies at Intel Corp. from 2001 to 2002. Her research interests include spectrum sliced WDM using incoherent sources for passive optical networks; semiconductor and erbium-doped optical amplifiers and their dynamics; radio over fiber; and in wireless communications, high performance, reduced complexity receivers for ultra-wide-band systems employing optical processing.